JGR Solid Earth

RESEARCH ARTICLE
10.1029/2019JB019301

Effusion Rate Evolution During Small-Volume Basaltic Eruptions: Insights From Numerical Modeling

A. Aravena [1], R. Cioni[1], D. Coppola[2], M. de' Michieli Vitturi[3], A. Neri[3], M. Pistolesi[4], and M. Ripepe[1]

[1]Dipartimento di Scienze della Terra, Università di Firenze, Florence, Italy, [2]Dipartimento di Scienze della Terra, Università di Torino, Torino, Italy, [3]Istituto Nazionale di Geofisica e Vulcanologia, Sezione di Pisa, Pisa, Italy, [4]Dipartimento di Scienze della Terra, Università di Pisa, Pisa, Italy

Key Points:
- The effects of magma source and feeding dike properties on the evolution of small-volume effusive eruptions are studied numerically
- Total erupted mass is mainly controlled by magma reservoir conditions (in particular, dimensions and overpressure) prior to the eruption
- Different types of effusion rate curves were modeled, classified, and compared with the effusion rate trends defined in the literature

Supporting Information:
- Supporting Information S1

Correspondence to:
A. Aravena,
alvaro.aravenaponce@unifi.it

Citation:
Aravena, A., Cioni, R., Coppola, D., de' Michieli Vitturi, M., Neri, A., Pistolesi, M., & Ripepe, M. (2020). Effusion Rate Evolution During Small-Volume Basaltic Eruptions: Insights From Numerical Modeling. *Journal of Geophysical Research: Solid Earth*, *124*, e2019JB019301. https://doi.org/10.1029/2019JB019301

Received 25 DEC 2019
Accepted 1 MAY 2020
Accepted article online 13 MAY 2020

Abstract The temporal evolution of effusion rate is the main controlling factor of lava spreading and emplacement conditions. Therefore, it represents the most relevant parameter for characterizing the dynamics of effusive eruptions and thus for assessing the volcanic hazard associated with this type of volcanism. Since the effusion rate curves can provide important insights into the properties of the magma feeding system, several efforts have been performed for their classification and interpretation. Here, a recently published numerical model is employed for studying the effects of magma source and feeding dike properties on the main characteristics (e.g., duration, erupted mass, and effusion rate trend) of small-volume effusive eruptions, in the absence of syn-eruptive magma injection from deeper storages. We show that the total erupted mass is mainly controlled by magma reservoir conditions (i.e., dimensions and overpressure) prior to the eruption, whereas conduit processes along with reservoir properties can significantly affect mean effusion rate, and thus, they dramatically influence eruption duration. Simulations reproduce a wide variety of effusion rate trends, whose occurrence is controlled by the complex competition between conduit enlargement and overpressure decrease due to magma withdrawal. These effusion rate curves were classified in four groups, which were associated with the different types described in the literature. Results agree with the traditional explanation of effusion rate curves and provide new insights for interpreting them, highlighting the importance of magma reservoir size, initial overpressure, and initial width of the feeding dike in controlling the nature of the resulting effusion rate curve.

1. Introduction

Effusion rate is a primary factor for determining the dynamics and evolution of effusive eruptions, the way in which lavas spread around volcanic areas, the lava emplacement conditions, and the resulting length and morphology of lava flows (Baloga & Pieri, 1986; Pinkerton & Wilson, 1994; Blake & Bruno, 2000; Calvari et al., 2003; Harris et al., 2007; Harris & Rowland, 2009; Malin, 1980; Tallarico et al., 2006; de' Michieli Vitturi & Tarquini, 2017). Hence, effusion rate represents a primary parameter in the assessment and mapping of the hazards and risks associated with this type of eruptions (Connor et al., 2012; Vicari et al., 2011). The temporal evolution of effusion rate defines the so-called effusion rate curve. During an effusive eruption, effusion rate may vary over three orders of magnitude, and a typical temporal sequence has been suggested, with an initial increasing trend from low values during the first minutes or hours, and a gradual decrease toward the end of the eruption (Coltelli et al., 2007; Harris et al., 2000; Harris et al., 2011; Swanson et al., 2014; Wadge, 1981). However, several case studies have shown a largely variable pattern for the temporal evolution of effusion rate where in many cases the initial increasing trend is unclear, the effusion rate exhibits a pulsating behavior, and/or the final stages are characterized by a nearly constant or even increasing trend (Harris et al., 2000; Harris et al., 2011; Harris & Neri, 2002; Lautze et al., 2004; Ripepe et al., 2015; Ripepe et al., 2017; Steffke et al., 2011). Harris et al. (2000) analyzed the evolution of effusion rate in several effusive eruptions and identified two different trends (Types I and II; Figure 1). Two additional effusion rate trends were then added by Harris et al. (2011) (Types III and IV; Figure 1). In particular, Type I trends are characterized by an increasing phase at the onset of the eruption and a longer phase of effusion rate decrease (i.e., similar to the effusion rate curve described by Wadge (1981)) and have been related to tapping of a pressurized magma volume. Type II trends present relatively stable and low effusion rates and have been interpreted as associated with non-pressurized overflow from summit craters. Type III trends are characterized

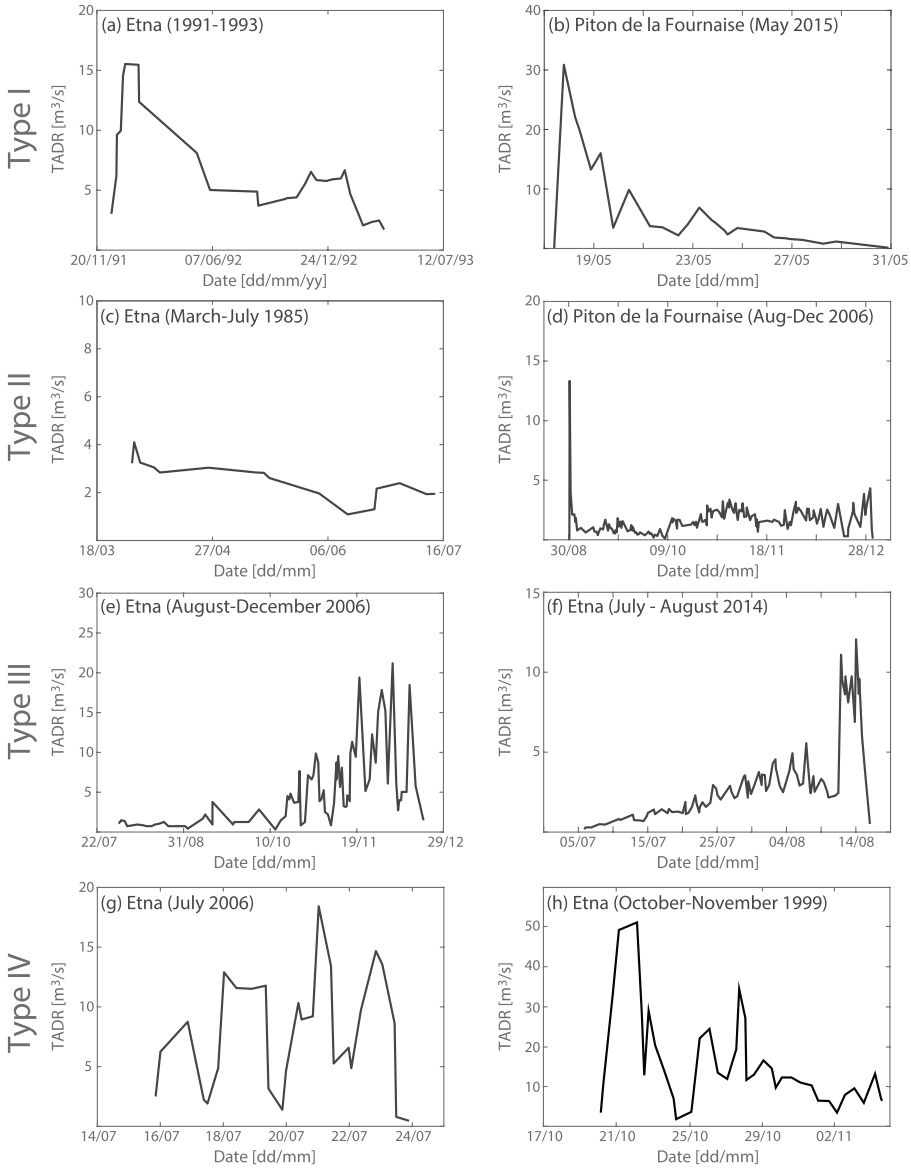

Figure 1. Examples of the different types of effusion rate curves identified in the literature. The data associated with these curves are satellite-derived time-averaged discharge rates (TADR). Modified from Coppola et al. (2009), Coppola et al. (2017), and Harris et al. (2011).

by increasing effusion rates with time and have been related to the ascent of a magma batch which pushes outside a shallower volume of degassed magma (Harris et al., 2011). Finally, Type IV trends present an oscillatory behavior, presumably related to fast ascent of multiple magma batches. Additionally, decreasing trends of effusion rate have been observed at Piton de la Fournaise, Etna, and Tolbachik volcanoes, among other case studies (Coppola et al., 2009; Coppola et al., 2019; Harris et al., 2011; Kubanek et al., 2017). Considering the rapid decrease of effusion rate and the eventual absence of reliable data for the waxing phase, these trends have been occasionally classified as Type I events (e.g., the 1983, 1986–1987, and 2002–2003 eruptions at Etna, and the 1984 eruption at Krafla; Harris et al., 2000; Harris et al., 2011). Because the variability of the observed effusion rate curves has been attributed to differences in the overpressure evolution of the magma source, the resulting trend would be influenced by the eventual magma influx in the reservoir, by modifications in the injected magma properties, and by several complex conduit processes (Aravena, Cioni, de' Michieli Vitturi, Pistolesi, et al., 2018; Calvari et al., 2010;

Clocchiatti et al., 2004; Coppola et al., 2017; Harris et al., 2011; La Spina et al., 2016; Piombo et al., 2016; Ripepe et al., 2009). In this sense, some recent works focused on modeling the evolution of effusion rate during basaltic eruptions (Aravena, Cioni, de' Michieli Vitturi, Pistolesi, et al., 2018; Piombo et al., 2016) giving evidence of the relevance of dike erosion and elastic deformation in controlling the effusion rate curve. Since the numerical model presented by Aravena, Cioni, de' Michieli Vitturi, Pistolesi, et al. (2018) is capable of reproducing a wide variety of effusion rate curves, important hints into the relationships between the properties of the volcanic system and the resulting effusion rate curves can be derived by developing a systematic analysis of modeling results.

In this investigation, we used an updated version of the model presented by Aravena, Cioni, de' Michieli Vitturi, Pistolesi, et al. (2018) in order to perform a sensitivity analysis of the resulting effusion rate curves with respect to four variable input parameters (specifically magma reservoir dimensions, initial overpressure of the magma reservoir, feeding dike erosion coefficient, and initial dimensions of the feeding dike). The choice of this set of uncertain input parameters is based on their influence in conduit widening and in the evolution of reservoir overpressure during effusive events, which are the main processes controlling the evolution of effusion rate in the absence of syn-eruptive magma feeding from deeper reservoirs (Aravena, Cioni, de' Michieli Vitturi, Pistolesi, et al., 2018; Piombo et al., 2016). In this way, we studied the factors controlling the most important characteristics of small-volume effusive events, such as eruption duration, total erupted mass, and mean and maximum effusion rate. We remark that the application of sensitivity analysis techniques, as those performed in recent volcanology works (e.g., de' Michieli Vitturi et al., 2016; Scollo et al., 2008; Woodhouse et al., 2016), furnishes a statistical framework to explore the results of numerical models, providing valuable information about the relationships between variability of input parameters and model outputs. It is also important to note that here we consider as effusion rate the instantaneous effusion rate as defined by Harris et al. (2007) and, as a reference case, we consider a set of input parameters and constitutive equations valid for a typical small-volume basaltic effusive eruption, in the absence of syn-eruptive melt injection from deeper storages. In this investigation we also evaluated the effect of water content and magma reservoir depth by performing some additional test simulations. Furthermore, we classified the effusion rate trends in four groups using appropriate characterizing and clustering techniques, and we determined the most significant properties of the volcanic system that would lead to the development of the different types of effusion rate curves identified in this work. Finally, modeling results were compared with the interpretation of the different effusion rate trends reported in the literature (Harris et al., 2000; Harris et al., 2011; Wadge, 1981).

2. Methods

We performed a set of simulations using a slightly modified version of the model presented in Aravena, Cioni, de' Michieli Vitturi, Pistolesi, et al. (2018) (see supporting information Text S1), which is capable of describing the evolution of effusive eruptions by considering the coupled effect of conduit erosion and elastic deformation of the feeding dike, and time-dependent variations of magma source properties (e.g., reservoir overpressure). A detailed study of the evolution of conduit geometry during effusive eruptions is provided in Aravena, Cioni, de' Michieli Vitturi, Pistolesi, et al. (2018), as well as the analysis of the factors controlling elastic deformation and conduit erosion by fluid shear stress, which is in turn influenced by magma velocity, viscosity, and a proportionality constant (erosion coefficient, k_e). Model modifications are associated with the assumptions adopted to impose the dependence between magma reservoir overpressure and erupted mass (Anderson & Segall, 2011). In the former version of the model (Aravena, Cioni, de' Michieli Vitturi, Pistolesi, et al., 2018), we assumed that magma reservoir overpressure was a linear function of erupted mass, whereas here we adopt an expression to determine magma reservoir overpressure that considers the compressibility of magma and the elastic expansivity of the reservoir (Text S1; Anderson & Segall, 2011; Marti et al., 2000; Macedonio et al., 2005). The way in which magma withdrawal influences reservoir overpressure depends on its size, the initial overpressure and effusion rate. Effusion rate is in turn strongly affected by conduit dimensions, giving rise to a complex interaction dynamics between conduit enlargement and overpressure evolution. It is also worth stressing that the adopted model considers a critical effusion rate (q_c) for defining the eruption end. This lies on the assumption that, once the feeding conduit is opened, magma evacuation stops when the dissipation forces experienced in the conduit are sufficient to counterbalance the pressure and density contrasts between magma in the reservoir and the surrounding rocks (Aravena, Cioni, de' Michieli Vitturi, Pistolesi, et al., 2018). Here we assume that $q_c = 0.2$ m^3/s, which is

Table 1
Invariant Input Parameters Used in Numerical Simulations

Parameter (units)	Symbol	Value
Feeding dike length (m)	L	3,000
Rigidity of magma chamber host rocks (GPa)	μ_{r0}	10
Initial magma density (kg/m^3)	ρ_0	2,600
Melt injection rate (m^3/s)	q_{in}	0
Critical effusion rate (m^3/s)	q_c	0.2
Poisson ratio (-)	ν	0.3
Feeding dike rigidity (GPa)	μ_r	30
Water content (wt.%)	w_1	1.5
CO_2 content (wt.%)	w_2	0.04
Initial semi-major axis of feeding dike (m)	$R_a(0)$	50
Characteristic roughness (m)	l_r	0.05
Country rock yield strength (MPa)	τ_B	10

significantly lower than the mean effusion rate of the modeled events. The values adopted for a set of invariant input parameters are presented in Table 1, where we use the nomenclature employed in Aravena, Cioni, de' Michieli Vitturi, Pistolesi, et al. (2018). On the other hand, the constitutive equations used for describing a representative basaltic effusive eruption are shown in Table 2.

In order to develop a sensitivity analysis, we assume uniform probability distributions for the four variable input parameters described previously: (1) magma reservoir diameter ($X_1 = D_0$, from 0.4 to 1.0 km, giving rise to magma reservoir volumes between 0.033 and 0.524 km^3; please note that we assume a spherical magma reservoir), (2) initial overpressure of the magma reservoir ($X_2 = p_{0i}$, from 5 to 25 MPa), (3) feeding dike erosion coefficient ($X_3 = k_e$, from 0 to 0.1), and (4) initial semi-minor axis of the feeding dike cross section ($X_4 = R_b(0)$, from 0.15 to 0.4 m; while the semi-major axis of the 3,000-m-long feeding dike cross section is fixed and equal to 50 m). It is also worth stressing that modifications in the erosion coefficient can be assumed as variations in feeding dyke roughness and/or yield strength (Aravena, Cioni, de' Michieli Vitturi, Pistolesi, et al., 2018; Macedonio et al., 1994). The initial semi-minor axis of the feeding dike is a parameter difficult to constrain and can be strongly influenced by structural settings, the dynamics of dyke opening, and the eventual occurrence of low-intensity explosive activity during early phases of effusive eruptions, as observed in some case studies (Harris et al., 2011; Kubanek et al., 2017). We studied the effects of the four input parameters described previously on five output variables: (1) mean effusion rate (Y_1), (2) maximum effusion rate (Y_2), (3) eruption duration (Y_3), (4) total erupted mass (Y_4), and (5) t_{50}/t_{100} (Y_5), where t_k represents the time required to evacuate the k percent of the total erupted mass (i.e., t_{100} represents eruption duration). Please note that some of the studied output parameters are interdependent such as mean eruption rate, which is defined as the ratio of erupted mass and eruption duration. In any case, we remark that this does not limit the applicability of the sensitivity analysis performed here. As sensitivity parameters, we calculated the first order (S_{ij}) and total-effect (T_{ij}) sensitivity indexes (Saltelli, 2002; Sobol, 2001):

$$S_{ij} = \frac{\mathrm{Var}\left(\mathrm{E}\left(Y_j|X_i\right)\right)}{\mathrm{Var}\left(Y_j\right)}, \tag{1}$$

$$T_{ij} = \frac{\mathrm{E}\left(\mathrm{Var}\left(Y_j|X_{\sim i}\right)\right)}{\mathrm{Var}\left(Y_j\right)}, \tag{2}$$

where X_i is the *i*th variable input parameter, Y_j is the *j*th output parameter, Var(·) is unconditional variance, E(·) is unconditional expectation, Var(·|·) is conditional variance, E(·|·) is conditional expectation, and $X_{\sim i}$ represents the set of all variable input parameters but X_i. Thus, S_{ij} represents the fraction of the output variability (Y_j) only attributed to the variability of the input parameter X_i (in other words, it measures the variance reduction in Y_j if X_i is fixed). On the other hand, T_{ij} measures the contribution to the output variance (Y_j) associated with the variable input parameter X_i, including all the interactions with other model inputs (in other words, it represents the variance left in the output parameter Y_j if all the inputs but X_i are fixed).

Additionally, using the same set of simulations and some complementary results, the development of different types of effusion rate curves was studied, as well as their controlling factors. For applying an objective classification criterion, effusion rate curves were divided in different groups by using appropriate characterizing and clustering strategies (see Text S2). For that, effusion rate curves were normalized in both axes, and for

Table 2
Constitutive Equations Used in Numerical Simulations

Constitutive equation	Model
Melt viscosity	Giordano et al. (2008)
Effect of crystals	Costa (2005)
Effect of bubbles	Costa et al. (2007)
Water and CO_2 solubility	Henry's law (La Spina et al., 2015)[a]
Crystallization	alphaMELTS calibration (Smith & Asimow, 2005)
Outgassing model	Darcy's law[b]
Exsolved gas equations of state	Ideal gas
Equations of state for crystals, melt, and dissolved water	Mie-Gruneisen equations (Le Métayer et al., 2005)

[a]The coefficients used to compute water solubility and CO_2 solubility, which are obviously different, were defined following La Spina et al. (2015). [b]Darcian permeability (k_1) is calculated considering a throat-bubble size ratio (f_{tb}) of 0.3, a tortuosity factor (m) of 4.0, and an average bubble size (r_b) calculated from bubble number density (N_d, equal to 10^8 m^{-3}) following Degruyter et al. (2012).

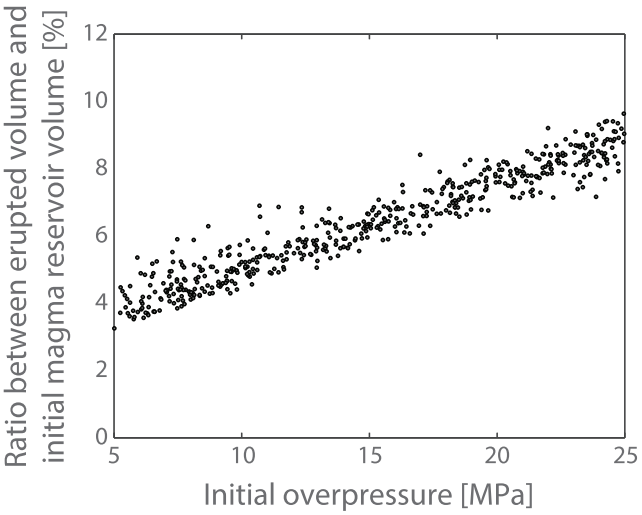

Figure 2. Ratio between modeled volume of erupted magma and initial magma reservoir volume, as a function of initial overpressure in the magma reservoir.

each pair of normalized curves, we computed the mean value of the Euclidean distance between them, obtaining a measure of their similarity degree (see Text S2 and Figure S1). Then, we hierarchically clustered the normalized effusion rate curves by using these similarity measures, where the optimal number of clusters was determined using the elbow method (see Text S2 and Figures S2–S3).

Finally, although the systematic analysis of the influence of magma reservoir depth and volatile content is beyond the objectives of this work, some test simulations are presented for illustrating the effect of these variables in modeling results. We also tested the effect of feeding dike rigidity and low-rate injection of melt in the magma reservoir (i.e., $q_{in} < 1$ m^3/s, consistent with estimates of long-term magma injection in some natural cases; Allard, 1997; Burton et al., 2009; Harris & Stevenson, 1997; Harris et al., 2011; Wadge & Guest, 1981), but because both parameters showed a negligible influence on effusion rate curves, they were excluded from the analysis presented here. Other non-considered parameters able to influence the resulting effusion rate curves are temporal modifications in magma properties (e.g., temperature and composition), high-rate injection of melt into the reservoir from deeper storages (e.g., $q_{in} > 5$ m^3/s), and the adoption of different shapes for magma reservoir, which has shown an important effect on reservoir compressibility and thus on the evolution of overpressure as magma is withdrawn (Amoruso & Crescentini, 2009; Anderson & Segall, 2011). We thus remark that the applicability field of our results is restricted to small-volume, basaltic, effusive events, fed by a compositionally homogeneous magma reservoir and in the absence of syn-eruptive melt injection from deeper storages.

3. Results

The results associated with 530 simulations exhibit a wide variety of effusion rate curves. They present maximum values of effusion rate between ~2.5 and >400 m^3/s, while mean effusion rate ranges from ~0.9 to ~260 m^3/s. The duration of simulated eruptions varies between ~1.6 and ~170 days, whereas the resulting erupted mass ranges from ~3.9×10^9 to ~1.3×10^{11} kg (i.e., erupted volume from ~1.6×10^6 to ~5.0×10^7 m^3). The erupted volumes derived from these simulations represent between 3% and 10% of the initial magma reservoir volume, and as expected, the largest values are associated with highly over-pressurized reservoirs (Figure 2). The linear relationship observed in Figure 2 is related to the limited magma compressibility that characterizes the reservoir in our numerical simulations. This is a consequence of the magma reservoir conditions assumed here, with low contents of CO_2 and water contents unable to induce H_2O exsolution at reservoir pressure. We also highlight that, because the eruption end is defined by adopting a criterion based on a critical effusion rate, the reservoir overpressure associated with eruption shutdown is also influenced by conduit dimensions during final stages of effusive eruptions. Thus, initial conduit width and erosion processes are additional factors able to influence eruption shutdown and thus the resulting erupted mass.

The results derived from a sensitivity analysis are presented in Figures 3 and 4. The observed variabilities in maximum and mean effusion rates are largely controlled by the prescribed variations in magma reservoir dimensions, initial overpressure, and erosion coefficient, while they are only slightly affected by variations in initial dike dimensions (at least within the variation ranges adopted here; Figures 3a-3h and 4). On the other hand, eruption duration variability is mainly controlled by the adopted variability of erosion coefficient (Figures 3i-3l), and it also exhibits a strong effect associated with the interaction between input parameters (as revealed by the value of $\sum_{i=1}^{4} S_{i3}$, which is significantly lower than 1.0; Figure 4a). The variability of total erupted mass is mainly controlled by changes in the dimensions of the magma reservoir (Figures 3m-3p and 4), while a minor effect is exerted by the prescribed variations in initial overpressure (Figure 4a). Finally, the major controlling factors of the observed variability of t_{50}/t_{100} are the prescribed variabilities of magma reservoir dimensions and erosion coefficient (Figures 3q-3t and 4).

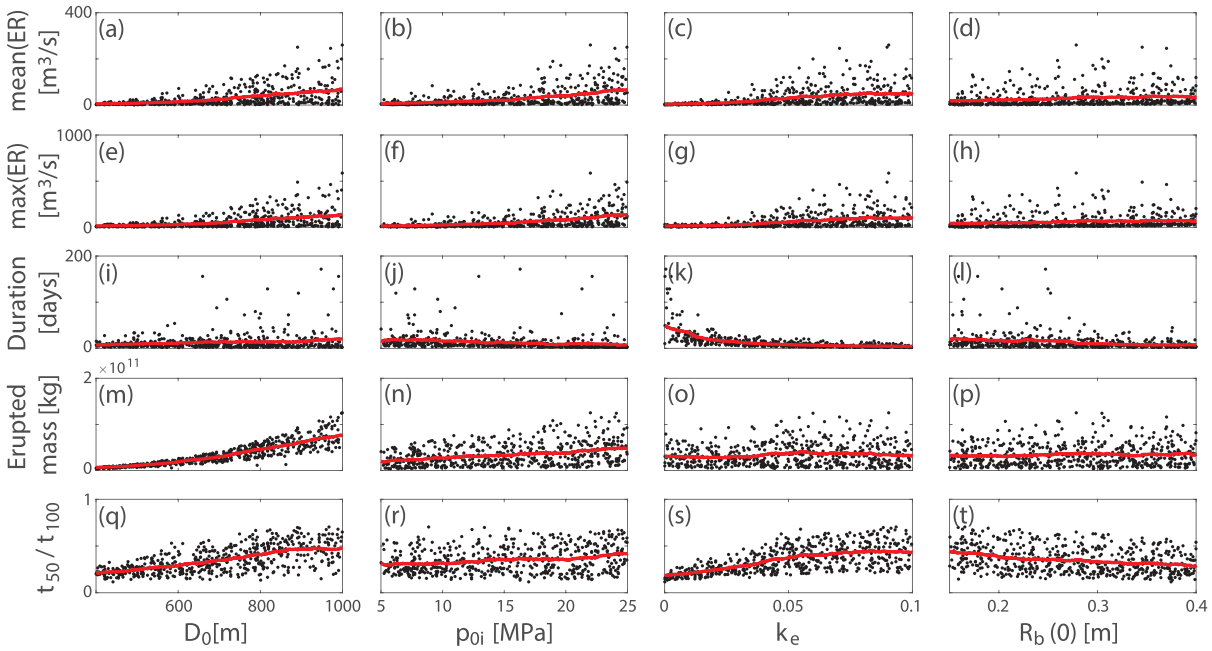

Figure 3. Results derived from the sensitivity analysis: relationship between input parameters and output variables. The variable input parameters are magma reservoir diameter (D_0), initial overpressure of the magma reservoir (p_{0i}), feeding dike erosion coefficient (k_e), and initial semi-minor axis of the feeding dike, $R_b(0)$, while the studied output parameters are maximum and mean effusion rate (ER), eruption duration, total erupted mass, and t_{50}/t_{100}, where t_k represents the time required to evacuate the k percent of the total erupted mass.

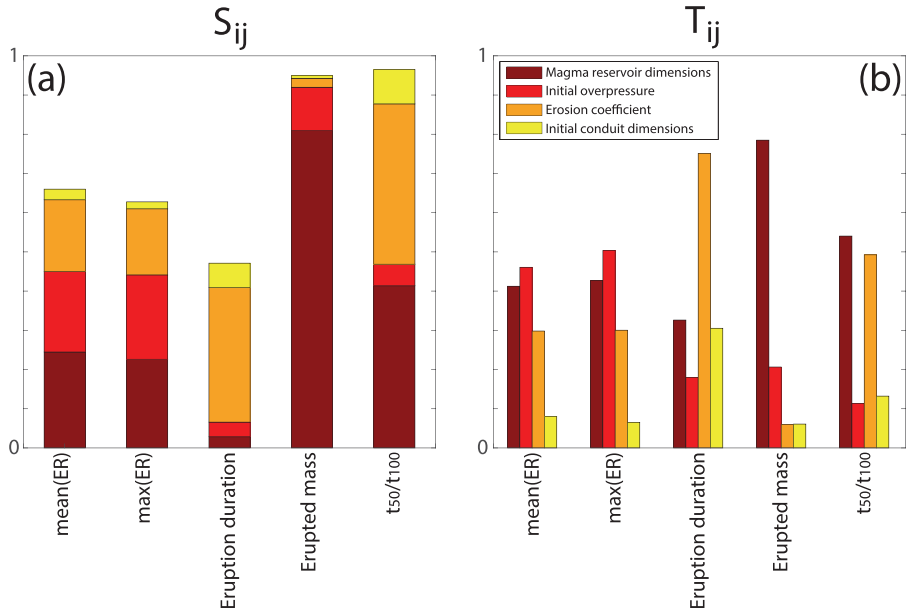

Figure 4. Results derived from the sensitivity analysis. (a) First order sensitivity index (equation 1). (b) Total effect sensitivity index (equation 2). The variable input parameters are magma reservoir diameter (D_0), initial overpressure of the magma reservoir (p_{0i}), feeding dike erosion coefficient (k_e), and initial semi-minor axis of the feeding dike, $R_b(0)$, while the studied output parameters are maximum and mean effusion rate (ER), eruption duration, total erupted mass, and t_{50}/t_{100}, where t_k represents the time required to evacuate the k percent of the total erupted mass.

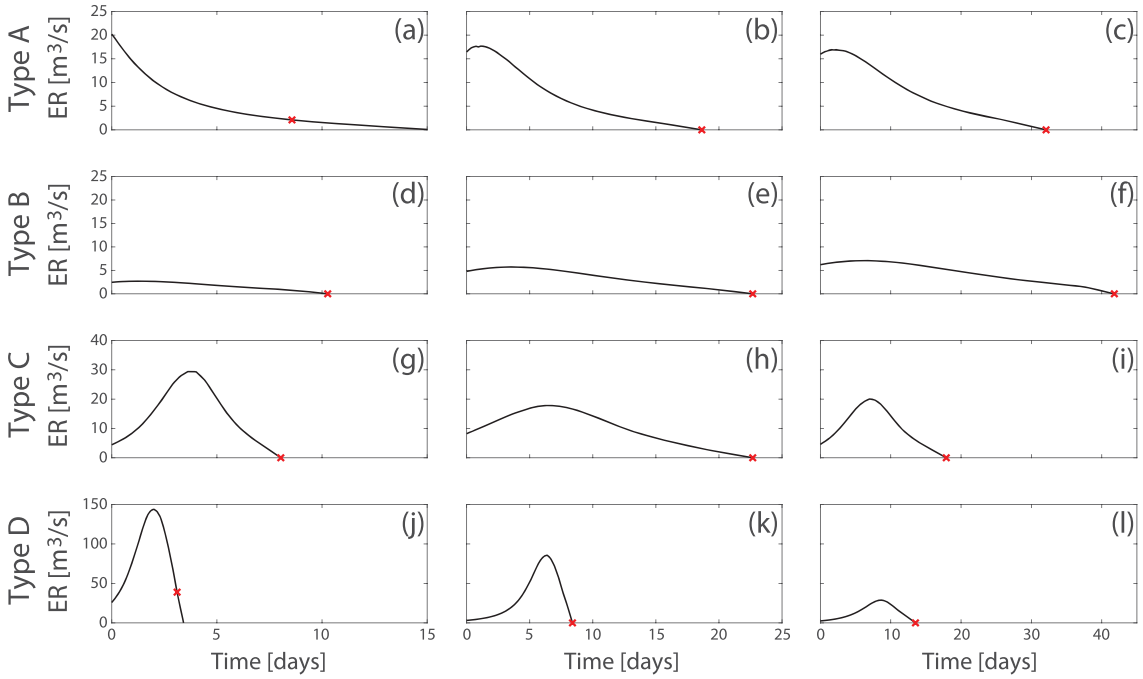

Figure 5. Examples of representative curves for the four types of effusion rate curves recognized in this work. In each panel, the red symbol would represent the eruption end if a pressure threshold of 70 MPa were considered for setting the eruption shutdown.

Using appropriate characterizing and clustering strategies (see Text S2), we recognized four types of effusion rate curves (Figure 5), whose main properties are the following:

1. Type A curves are characterized by clearly dominant decreasing tendencies (Figures 5a-5c), which result in low values of t_{50}/t_{100} (95% of simulations between 0.15 and 0.26; Figure 6d) and hence in an early peak in the effusion rate curve. These eruptions present relatively low effusion rates (mean values between ~1 and ~20 m^3/s, with 85% of simulations with mean effusion rates lower than 10 m^3/s) and highly variable results for duration (from ~2 to >100 days) and erupted mass (from 4.0×10^9 to 7.9×10^{10} kg, i.e., erupted volume between ~1.6×10^6 and ~3.2×10^7 m^3).
2. Type B is characterized by relatively low and, in some cases, nearly constant effusion rates (Figures 5d-5f). These simulations typically present mean values of effusion rate in the range between ~2 and ~27 m^3/s (2.5th and 97.5th percentiles, respectively) and standard deviations between ~1 and ~19 m^3/s (2.5th and 97.5th percentiles, respectively; Figures 6a and 6f), slightly higher than Type A. However, Type B presents significantly lower values of relative variability with respect to Type A (i.e., standard deviation divided by mean value), which ranges from 0.49 to 0.79 for Type B and from 0.66 to 1.42 for Type A. In general, the low effusion rate relates to relatively long events, with durations that frequently exceed 6 days. Additionally, t_{50}/t_{100} ranges between 0.24 and 0.35, while total erupted mass tends to be smaller than that observed in Groups C and D, with values between 3.9×10^9 and 9.0×10^{10} kg (Figure 6c, i.e., erupted volume from ~1.6×10^6 to ~3.6×10^7 m^3).
3. Type C includes effusive events with a clear peak near the middle of the eruption (t_{50}/t_{100} between 0.34 and 0.47; Figures 5g-5i and 6d), and relatively high mean effusion rates (Figure 6a). Type C eruptions present low durations (78% of simulations with values lower than 10 days) and highly variable values of erupted mass (ranging between 8.4×10^9 and 9.5×10^{10} kg, i.e., erupted volume from ~3.4×10^6 to ~3.8×10^7 m^3).
4. Type D is characterized by peaks of effusion rate during the final phases of the eruption (t_{50}/t_{100} between 0.46 and 0.70; Figure 6d), including eruptions with clear waxing and waning phases (Figures 5j-5l). These events present relatively high mean effusion rates (between 10 and >150 m^3/s), and typically short durations (72% of simulations present durations lower than 6 days). The total erupted mass tends to be larger

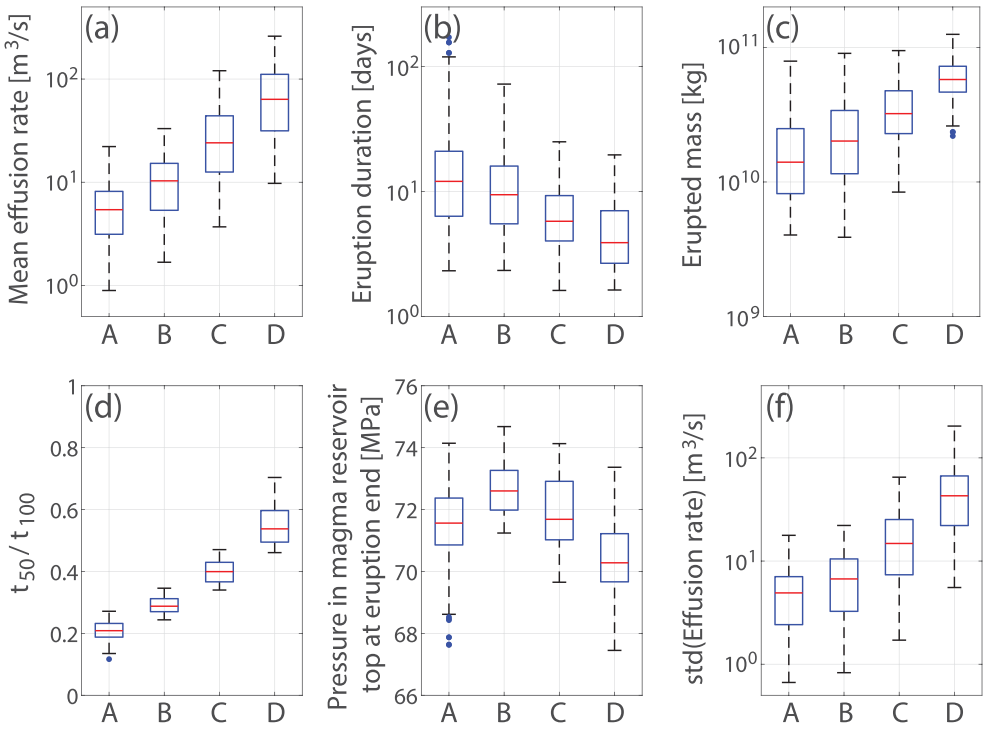

Figure 6. Box-plots of (a) mean effusion rate in log scale, (b) eruption duration in log scale, (c) erupted mass in log scale, (d) t_{50}/t_{100}, (e) pressure in magma reservoir top at eruption end, and (f) standard deviation of effusion rate in log scale, for the different types of effusion rate curve. In each box-plot, the red line indicates the median value, while the bottom and top edges of the box indicate the 25th and 75th percentiles, respectively. The dashed lines extend to the most extreme points not considered outliers.

than that observed in the other groups, ranging from 2.2×10^{10} to 1.3×10^{11} kg (Figure 6c, i.e., erupted volume between ~8.8×10^{6} and ~5.0×10^{7} m^3).

It is worth stressing that the adopted numerical model assumes that the evacuation of magma stops when the effusion rate drops below a critical effusion rate (q_c), which may occur either before or after reaching the lithostatic pressure (Aravena, Cioni, de' Michieli Vitturi, Pistolesi, et al., 2018). However, considering that a reservoir pressure far below the lithostatic value may induce instability conditions, collapse processes, and conduit closure (Aravena et al., 2017; Aravena, Cioni, de' Michieli Vitturi, & Neri, 2018; Macedonio et al., 1994), the eruption shutdown can be otherwise defined with the application of a critical reservoir pressure (p_c) (Marti et al., 2000). This modification would introduce some variations in the resulting effusion rate curves (Figure 5). In particular, for Type D curves, the events would be characterized by an abrupt drop of effusion rate at the end of the eruption, which can be significantly promoted by the low reservoir pressure typically reached during these events (Figure 6e). In fact, if we assume that p_c = 70 MPa (in our case ~6 MPa below lithostatic pressure), 40% of the Type D simulations would present a final phase characterized by an abrupt effusion rate drop, higher than 20 m^3/s. On the other hand, some eruptions grouped in Type A would be significantly shorter (Figure 5a). However, since they are characterized by gradual, long waning phases, this process would not imply an abrupt decrease in intensity at the end of these eruptions (in fact, if we assume that p_c = 70 MPa, the effusion rate drop would be lower than 3 m^3/s for all the simulations associated with Type A). Finally, since Types B and C do not produce dramatic overpressure drops (Figure 6e), the use of an overpressure threshold for setting the eruption shutdown would result in minor modifications for these events. The boxplots of the main characteristics of the different groups of effusion rate curves if an overpressure threshold were considered are presented in Figure S4.

Figures 7 and 8 show the conditions at which the different types of effusion rate curves are observed, as a function of magma reservoir dimensions, initial overpressure, erosion coefficient, and initial dimensions

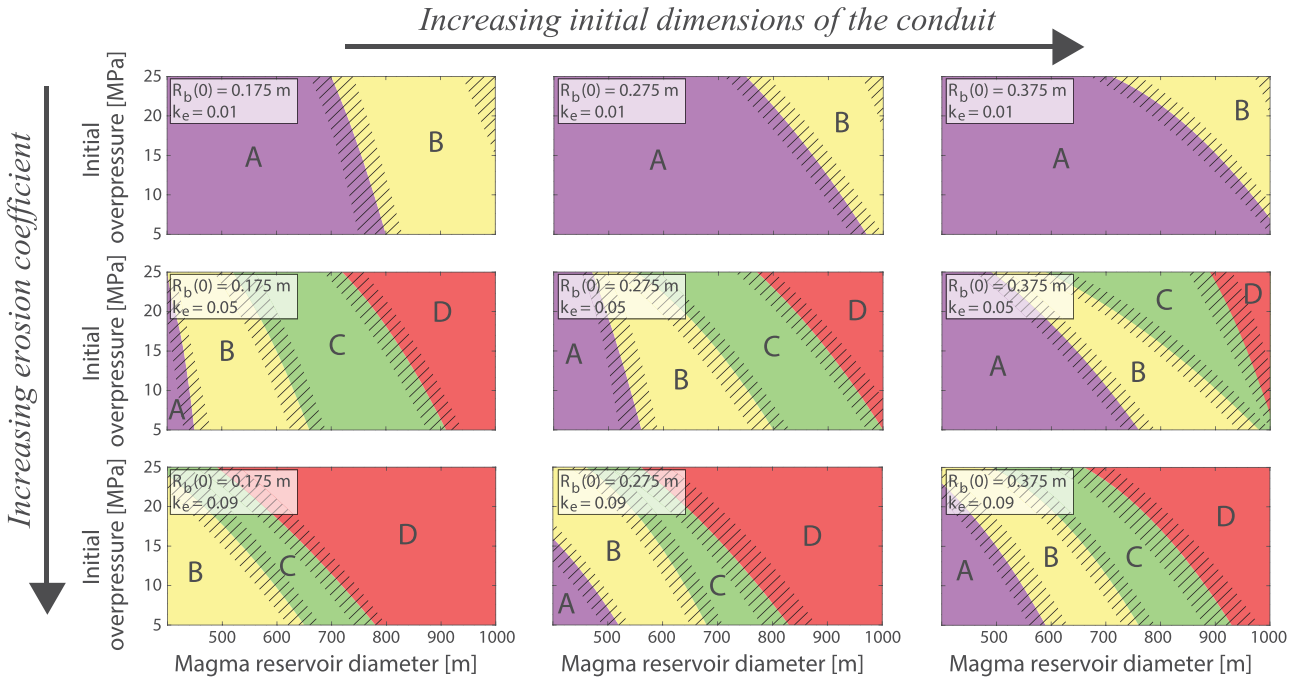

Figure 7. Conditions at which the different types of effusion rate curves are observed. Each panel is associated with fixed values of initial dimensions of the conduit, $R_b(0)$, and erosion coefficient (k_e), while the Cartesian axes of each panel are related to magma reservoir dimensions and initial overpressure. The transitional domains between two or more types of effusion rate curves are indicated by diagonal, black lines.

of the feeding dike. Each figure contains nine panels characterized by fixed values for two of the studied input parameters, while the remaining two input variables are represented in the Cartesian axes (the shaded areas with black, diagonal lines indicate the transition domains between two or more types of

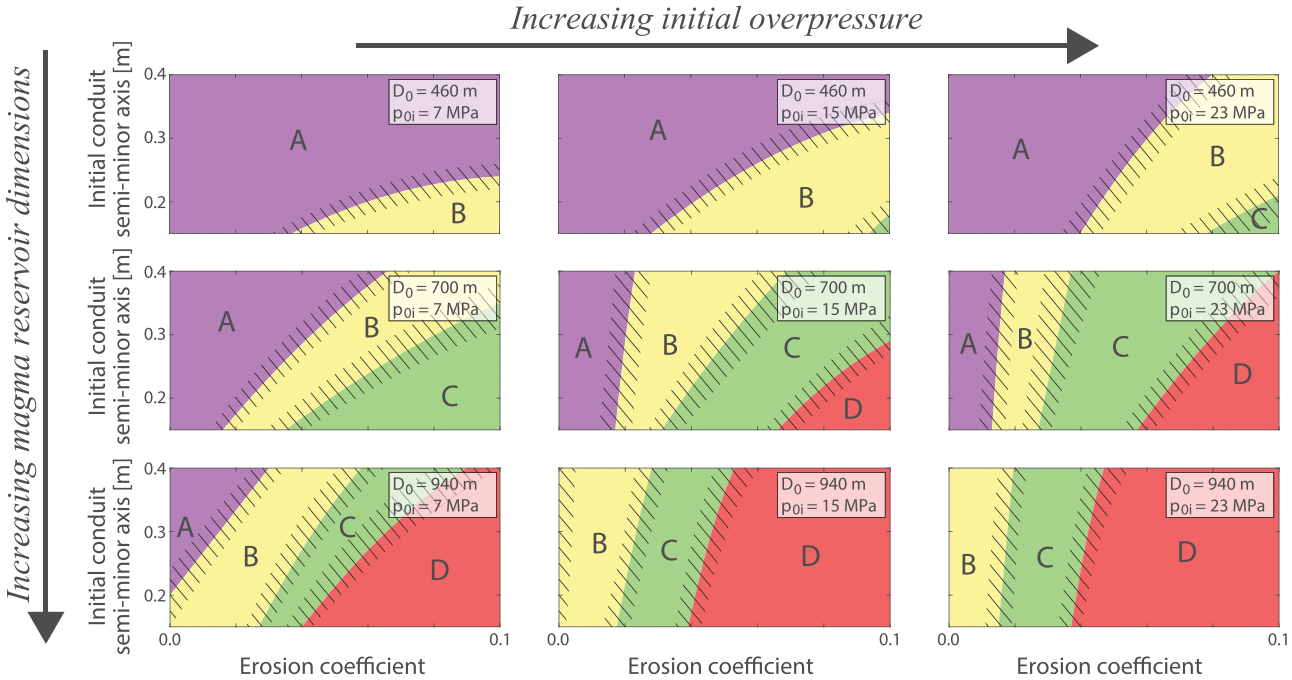

Figure 8. Conditions at which the different types of effusion rate curves are observed. Each panel is associated with fixed values of initial overpressure (p_{0i}) and magma reservoir dimensions (D_0), while the Cartesian axes of each panel are related to erosion coefficient and initial dimensions of the conduit. The transitional domains between two or more types of effusion rate curves are indicated by diagonal, black lines.

effusion rate curves). Results indicate that the development of the different types of effusion rate curves is influenced by strong interdependencies between the variable inputs considered in our simulations. Please note that, in this section, the values of variable input parameters are described in terms of their relative position within the prescribed variation ranges. Type A curves are typically observed for low values of erosion coefficient and small magma reservoirs, and they are also favored by large initial widths of the feeding dike (Figures 7 and 8). These conditions allow producing a relatively high effusion rate (>10 m^3/s for more than 70% of Type A simulations) during the initial phases of the eruption, with a rapid overpressure drop which may be favored by the presence of a low-volume reservoir. This fact, along with a weak feeding dike enlarging process, results in a decreasing trend of effusion rate. On the contrary, when moderate to high values of erosion coefficient and/or reservoir diameter (with respect to the prescribed variation ranges) are able to counteract or at least significantly delay the effusion rate decrease, Type B curves can be produced, which are also favored by the presence of narrow feeding dikes at eruption onset. In some cases, Type B curves exhibit nearly constant effusion rates during a significant portion of the eruption. This is strongly related to the presence of low initial overpressures in the magma reservoir (<10 MPa), while no correlations were found with respect to other variable input parameters. In fact, considering exclusively Type B curves with an initial overpressure in the magma reservoir between 5 and 10 MPa, the ratio between the standard deviation of effusion rate and its mean value is 0.60 ± 0.05, while this ratio is 0.71 ± 0.04 when the adopted range for initial magma reservoir overpressure is 20-25 MPa. On the other hand, intense erosion processes from the onset of the eruption (favored by high erosion coefficients, high initial overpressures, and/or large magma reservoirs with respect to the prescribed variation ranges) can result in a well-developed phase of effusion rate increase, producing Type C or D curves. The difference between them mainly lies on magma reservoir diameter, initial overpressure, and erosion coefficient (Figures 7 and 8). For Type D events, conduit erosion is so intense to reach very high effusion rates (e.g., >100 m^3/s), producing an abrupt magma withdrawal, the consequent overpressure drop, and an eruption shutdown characterized by a rapid decrease of effusion rate, in contrast to the gradual effusion rate decrease observed in Type C events.

It is worth noting here that the ranges assumed in this work for the input parameters are not related to a specific volcanic system, and the deduction of particular numerical constrains for developing the different types of effusion rate curves for a given case study would require the inclusion of more detailed information of the specific volcanic system (e.g., depth and size of the reservoir, nature of the ascending magma, and critical overpressure needed to trigger volcanic events). For instance, the presence of a shallower magma reservoir or an increase in magma water content would favor the occurrence of clear peaks of effusion rate, reducing eruption duration, increasing mean effusion rate and t_{50}/t_{100} (Figure S5), and thus strongly displacing the fields associated with the different types of effusion rate curves presented in Figures 7 and 8.

4. Discussion

The factors controlling the evolution of effusion rate during basaltic eruptions have been addressed by adopting a numerical model able to describe the temporal evolution of effusive eruptions (Aravena, Cioni, de' Michieli Vitturi, Pistolesi, et al., 2018). We performed a set of numerical simulations considering four variable input parameters: size of the magma reservoir, initial overpressure, initial dimensions of the feeding dike, and erosion coefficient. Considering the limited set of variable input parameters and their prescribed variability ranges, the applicability field of the simulations described here is limited to small-volume effusive eruptions, in the absence of chemical zonation in the magma reservoir and without consideration of melt injection from deeper storages. In this section, we discuss the results associated with the sensitivity analysis performed in this work and with the study of the different types of effusion rate curves derived from numerical modeling, including their comparison with the effusion rate trends defined in the literature. Finally, we present the volcanological implications derived from this work.

4.1. Sensitivity Analysis

The temporal evolution of effusion rate during small-volume effusive eruptions is controlled by the properties of the feeding system (i.e., size of the magma reservoir and initial overpressure) and by the characteristics of the dike (i.e., initial dimensions and erosion coefficient). In fact, they all influence the balance between dike widening and the withdrawal-driven overpressure decrease, and thus, they control the most

important characteristics of the resulting effusive eruptions (e.g., duration, maximum effusion rate, and total erupted mass).

In particular, numerical results suggest that erupted mass is mainly controlled by magma reservoir conditions, while conduit processes do not seem to induce significant modifications in this output parameter. Because erupted mass is positively correlated with magma reservoir dimensions and initial overpressure, in the absence of significant variations in the supply dynamics of deeper magma, results could support the idea that the time interval between two successive eruptions can represent an indicator of the maximum mass of magma that is likely to be discharged (Branca & Del Carlo, 2005; Calvari et al., 2003; Cioni et al., 2008). On the other hand, conduit processes along with reservoir properties can influence magma withdrawal rate, and thus, they dramatically affect eruption duration, maximum and mean effusion rate, and the cumulative curve of erupted mass. In this sense, we stress that highly consistent dependencies between conduit dynamics and eruption duration and intensity have been identified in explosive events from numerical modeling (Colucci et al., 2014; Macedonio et al., 2005).

4.2. Effusion Rate Curves

Because the adopted numerical model is able to reproduce different trends of effusion rate, it can be employed for data inversion in order to analyze specific volcanic events through the study of their temporal evolution. Based on the application of appropriate characterizing and clustering methods, the effusion rate curves were grouped in four categories. The four groups identified here cannot be directly linked to the different types defined in the literature (Harris et al., 2000; Harris et al., 2011; Wadge, 1981). This is a consequence of the restricted set of variable input parameters considered here (e.g., we did not consider injection of deeper magma, or variations in magma composition) and their bounded variability ranges, which limit the spectrum of the effusion rate curves modeled in this investigation. Moreover, the types of effusion rate curves defined in the literature are based on the analysis of information characterized by poorly constrained periods of observational data (Coppola et al., 2009;Harris et al., 2000 ; Harris et al., 2011) or by too low acquisition frequency to record short-period variations (Harris et al., 2000; James et al., 2010; Lautze et al., 2004). Although the comparison between modeled effusion rate curves and those defined in the literature presents intrinsic practical limitations, some similarities can still be proposed, which can be useful to interpret the first order variations observed during effusive eruptions.

In particular, because of the presence of clear waxing and waning phases and the typical ranges of modeled effusion rate, Type C can be associated with Type I of Harris et al. (2000). These curves are expected in eruptions that experience a significant conduit enlargement able to produce a relatively long phase of increase of effusion rate from the eruption onset, which is favored by the presence of high erosion coefficients, high initial overpressures, and/or large magma reservoirs, while the subsequent effusion rate decrease is controlled by the gradual pressure drop derived from magma withdrawal. These results are consistent with the traditional interpretation of Type I curves, that is, the emission of a pressurized magma volume (Harris et al., 2000; Wadge, 1981). However, this condition would not be necessarily expected if Type I eruptions (Harris et al., 2000; Harris et al., 2011) were associated with A-type eruptions. In fact, numerical results highlight that decreasing trends of effusion rate (i.e., Type A), which have been frequently classified as Type I eruptions (e.g., the 1983, 1986–1987, and 2002–2003 eruptions at Etna, and the 1984 eruption at Krafla; Harris et al., 2000; Harris et al., 2011), are not necessarily related to a highly pressurized system, and they may reflect a rapid initial overpressure decrease derived from a particularly efficient magma withdrawal. In this sense, in addition to the overpressure of the magma reservoir, we can suggest other conditions able to drive a particularly efficient magma ascent since early stages of effusive eruptions, such as (1) the involvement of volatile-rich, low-crystallinity, low-viscosity magmas; (2) small depths of the feeding system; and/or (3) efficient dike opening (e.g., produced by minor explosive activity), as highlighted in this work.

On the other hand, because Type B events exhibit low effusion rates with a limited temporal variability, they could be associated with Type II eruptions (Harris et al., 2000). These effusion rate curves are particularly similar for numerical simulations associated with low values of initial overpressure in the magma reservoir, as remarked in section 3, which is consistent with the overflow of a non-pressurized system, as commonly claimed for this category (Harris et al., 2000; Harris et al., 2011).

Finally, considering the dominant increasing tendency of effusion rate, the abrupt intensity drop just prior to the eruption end and the presence of similar values of effusion rate, Type D eruptions could be associated with Type III events (Harris et al., 2011). In this sense, it is also worth noting that the abrupt decrease of effusion rate observed in Type D events could be amplified by the occurrence of a collapse-dominated eruption shutdown, which is particularly likely for this group of eruptions (Figure 6e). Type D curves are expected for events characterized by small initial widths of the feeding dike, high initial overpressures, and/or large reservoir diameters. This result provides an alternative, non-exclusive explanation for Type III eruptions, which does not require temporal modifications in the magma source and/or compositional zoning of the reservoir, in contrast to the traditional interpretation (Harris et al., 2011). It is however important to highlight that the eruption durations associated with our Type D curves are significantly lower than those observed in nature (Harris et al., 2011). In fact, the latter present long low-intensity phases prior to the gradual increase of effusion rate and the subsequent abrupt final decrease (Figure 1).

The development of Type IV trends of Harris et al. (2011) probably requires the involvement of temporal modifications of the supply rate in the magma reservoir (Costa et al., 2007; Melnik & Sparks, 2005), and they were not reproduced by the set of input parameters adopted here. In this regard, although magma injection rates comparable with long-term estimates for natural cases (i.e., <1 m^3/s) are not capable of inducing dramatic changes in the eruptive dynamics, geological data suggest that these processes may occur at much higher rates when they are triggered by the rapid effusion of large volumes of magma (e.g., the February 2005 eruption at Piton de la Fournaise; Coppola et al., 2009; Coppola et al., 2017), significantly affecting the temporal evolution of effusion rate, as stressed in Aravena, Cioni, de' Michieli Vitturi, Pistolesi, et al. (2018).

4.3. Volcanological Implications

The evolution of effusion rate during effusive eruptions is controlled by the competition between conduit widening and overpressure decrease, which are influenced not only by the ascending magma properties but also by the characteristics of surrounding rocks and their interaction dynamics. Numerical modeling suggests that volcanoes are likely to generate preferentially certain types of effusion rate curves, as a function of depth and dimensions of the magma reservoir, the critical overpressure needed to trigger dike opening, and mechanical properties of the country rocks. Other plausible controlling factors are associated with deep feeding mechanisms and the dynamics of stress reorganization after the injection and/or evacuation of magma (Coppola et al., 2017; Got et al., 2013). We suggest that long-term variations in the behavior of a given volcano can be controlled by changes in the feeding system and in the nature of the volcanic edifice, which are likely to occur after important volcanic events. For instance, recently, Mt. Etna has experienced at least three periods characterized by a marked shift in effusion style (Coltelli et al., 2007; Harris et al., 2011): (1) 1983–1993, characterized by less frequent but longer effusive events (Types I and II); (2) 1994–1999, which represents a transitional period; and (3) 2000–2010, characterized by more frequent but shorter eruptions with higher effusion rate and periods of explosive activity (Types I, III, and IV). This has been interpreted as the result of modifications in the rheology of the ascending magma (Clocchiatti et al., 2004; Harris et al., 2011), favoring the occurrence of events with more efficient magma ascent. In agreement with our results, these conditions would in fact modify the long-term behavior of the volcanic system, with the unlikely occurrence of Type II events during the third period. Moreover, the preferential occurrence of high effusion rate events in this period, along with the presence of magma with lower viscosity, could lead to a highly variable short-term dynamics in the deep injection of magma, resulting in effusion rate curves apparently dominated by high-rate injection of melt in the reservoir (e.g., Types III and IV), which were not observed in the previous periods (Harris et al., 2011).

On the other hand, in some volcanoes, a clear dependence has been identified between vent location and the resulting eruption dynamics (e.g., summit eruptions versus lateral events at Piton de la Fournaise and Etna volcanoes; Andronico et al., 2005; Coppola et al., 2009; Harris et al., 2011; Neri et al., 2005; Neri & Acocella, 2006). In particular, at Piton de la Fournaise, Coppola et al. (2009) proposed that the relationship between vent location and the characteristic overpressure of volcanic events (and thus the resulting curve of effusion rate) is controlled by dike opening and propagation dynamics, while Etna volcano shows vent position-controlled differences in the ascending magma properties and thus in the resulting eruptive

dynamics (Andronico et al., 2005; Behncke & Neri, 2003; Clocchiatti et al., 2004; Neri & Acocella, 2006; Neri et al., 2005). In fact, as described here, both magma properties (e.g., water content) and initial reservoir overpressure are able to exert an important effect on magma ascent, on the competition between dike widening and the withdrawal-driven overpressure decrease, and thus on the expected effusion rate curve. Accordingly, a detailed study of the expected ascent conditions (e.g., initial overpressure, country rock mechanical properties, structural settings, magma properties, and eventual zonations in the reservoir, among others) in different zones of a given volcanic system is potentially able to provide important data for the characterization of the expected volcanic events as a function of vent location (e.g., duration and mean effusion rate). Considering that the temporal evolution of effusion rate is the main factor controlling the dynamics of lava spreading during effusive events and the intrinsic relevance associated with vent position in the expected zones of lava inundation, a detailed analysis of the relationship between the characteristics of effusion events (e.g., duration and mean effusion rate) and vent location in a specific volcanic system may provide key information for the assessment of volcanic hazard. This is particularly critical when significant uncertainty is associated with vent position, as observed for example at Etna (Cappello et al., 2012) and Pacaya volcanoes (Rose et al., 2013).

5. Conclusions

In this work we simulate the temporal evolution of effusion rate during small-volume basaltic eruptions considering four variable input parameters (dimensions and overpressure of magma reservoir, feeding dike erosion coefficient, and initial dike width). Besides traditional interpretations of the observed effusion rate curves, these results highlight the effect of magma storage and conduit properties on the eruptive dynamics. The main findings derived from numerical modeling of small-volume effusive eruptions and the analysis of the resulting effusion rate curves are summarized below:

1. The total erupted mass in effusive eruptions is mainly controlled by the properties of the magma reservoir (i.e., dimensions and initial overpressure), while the effect of conduit processes seems to be negligible. Thus, in the absence of significant long-term variations in deeper magma supply, numerical results support the idea that the time interval between two successive events can represent an indicator of the maximum magma mass that is likely to be discharged.
2. Feeding dike characteristics (i.e., initial dimensions and erosion coefficient) along with reservoir properties can influence magma withdrawal rate, and thus, they significantly affect eruption duration, maximum and mean effusion rate, and the nature of the cumulative curve of erupted mass. Considering the limited influence of conduit processes on erupted volume, defined as the product between eruption duration and mean effusion rate, this implies that the effects of conduit dynamics on eruption duration and on mean effusion rate are negatively correlated.
3. The effusion rate curve of a given basaltic eruption is able to provide important insights for understanding the characteristics of the source of magma and conduit properties. In particular, Type C eruptions (i.e., characterized by a clear peak of effusion rate near the middle of the eruption and thus assumed as associated with Type I of Harris et al., 2000) are expected for events dominated by a significant erosion process from the onset of the eruption, able to increase moderately the effusion rate and lead to a later waning phase controlled by the overpressure decrease driven by magma withdrawal. Decreasing trends of effusion rate (i.e., Type A of this work), frequently classified as Type I eruptions, are not necessarily related to highly pressurized systems, as commonly claimed for Type I events, and they may reflect a rapid overpressure decrease derived from a particularly efficient magma withdrawal during eruption onset. Type B eruptions (i.e., characterized by relatively low and, in some cases, nearly constant effusion rates, and thus assumed at least partially as equivalent to Type II of Harris et al., 2000) are produced in events characterized by low initial overpressures and moderate erosion processes, consistent with the traditional interpretation of this type of effusion rate curve. Type D events (i.e., characterized by peaks of effusion rate during the final phases of the eruption and thus assumed as equivalent to Type III of Harris et al., 2011) are expected in eruptions with efficient erosion processes, favored by high initial overpressures and/or large reservoir diameters. Under our simulation conditions (i.e., without considering injection processes from deeper storages), effusion rate curves characterized by an oscillating behavior (e.g., Type IV of Harris et al., 2011) were not modeled.

4. Systematic variations in effusion rate curves of a given volcano over time can be interpreted as modifications in the feeding system and/or in the volcanic edifice.
5. Considering the importance of effusion rate evolution and vent position in the spreading dynamics of lava flows, a detailed study of their eventual relationships, as described for example at Piton de la Fournaise and Etna volcanoes, may provide key information for volcanic hazard assessment when significant uncertainty is associated with vent position.

Acknowledgments

We thank Benoit Taisne and an anonymous reviewer for their useful suggestions and comments. This paper is a theoretical work, and we do not present new field data. The conduit model adopted in order to describe effusive eruptions is available online (https://github.com/demichie/MAMMA) and also in the repository (associated with DOI: 10.5281/zenodo.3592813).

References

Allard, P. (1997). Endogenous magma degassing and storage at Mount Etna. *Geophysical Research Letters*, *24*(17), 2219–2222. https://doi.org/10.1029/97GL02101

Amoruso, A., & Crescentini, L. (2009). Shape and volume change of pressurized ellipsoidal cavities from deformation and seismic data. *Journal of Geophysical Research*, *114*, B02210. https://doi.org/10.1029/2008JB005946

Anderson, K., & Segall, P. (2011). Physics-based models of ground deformation and extrusion rate at effusively erupting volcanoes. *Journal of Geophysical Research*, *116*, B07204. https://doi.org/10.1029/2010JB007939

Andronico, D., Branca, S., Calvari, S., Burton, M., Caltabiano, T., Corsaro, R., et al. (2005). A multi-disciplinary study of the 2002–03 Etna eruption: Insights into a complex plumbing system. *Bulletin of Volcanology*, *67*(4), 314–330. https://doi.org/10.1007/s00445-004-0372-8

Aravena, A., Cioni, R., de' Michieli Vitturi, M., & Neri, A. (2018). Conduit stability effects on intensity and steadiness of explosive eruptions. *Scientific Reports*, *8*(1), 4125. https://doi.org/10.1038/s41598-018-22539-8

Aravena, A., Cioni, R., de' Michieli Vitturi, M., Pistolesi, M., Ripepe, M., & Neri, A. (2018). Evolution of conduit geometry and eruptive parameters during effusive events. *Geophysical Research Letters*, *45*, 7471–7480. https://doi.org/10.1029/2018GL077806

Aravena, A., de' Michieli Vitturi, M., Cioni, R., & Neri, A. (2017). Stability of volcanic conduits during explosive eruptions. *Journal of Volcanology and Geothermal Research*, *339*, 52–62. https://doi.org/10.1016/j.jvolgeores.2017.05.003

Baloga, S., & Pieri, D. (1986). Time-dependent profiles of lava flows. *Journal of Geophysical Research*, *91*(B9), 9543–9552. https://doi.org/10.1029/JB091iB09p09543

Behncke, B., & Neri, M. (2003). The July–August 2001 eruption of Mt. Etna (Sicily). *Bulletin of Volcanology*, *65*(7), 461–476. https://doi.org/10.1007/s00445-003-0274-1

Blake, S., & Bruno, B. (2000). Modelling the emplacement of compound lava flows. *Earth and Planetary Science Letters*, *184*(1), 181–197. https://doi.org/10.1016/S0012-821X(00)00278-8

Branca, S., & Del Carlo, P. (2005). Types of eruptions of Etna volcano AD 1670–2003: Implications for short-term eruptive behaviour. *Bulletin of Volcanology*, *67*(8), 732–742. https://doi.org/10.1007/s00445-005-0412-z

Burton, M., Caltabiano, T., Murè, F., Salerno, G., & Randazzo, D. (2009). SO2 flux from Stromboli during the 2007 eruption: Results from the FLAME network and traverse measurements. *Journal of Volcanology and Geothermal Research*, *182*(3–4), 214–220. https://doi.org/10.1016/j.jvolgeores.2008.11.025

Calvari, S., Lodato, L., Steffke, A., Cristaldi, A., Harris, A. J., Spampinato, L., & Boschi, E. (2010). The 2007 Stromboli eruption: Event chronology and effusion rates using thermal infrared data. *Journal of Geophysical Research*, *115*, B04201. https://doi.org/10.1029/2009JB006478

Calvari, S., Neri, M., & Pinkerton, H. (2003). Effusion rate estimations during the 1999 summit eruption on Mount Etna, and growth of two distinct lava flow fields. *Journal of Volcanology and Geothermal Research*, *119*(1-4), 107–123. https://doi.org/10.1016/S0377-0273(02)00308-6

Cappello, A., Neri, M., Acocella, V., Gallo, G., Vicari, A., & Del Negro, C. (2012). Spatial vent opening probability map of Etna volcano (Sicily, Italy). *Bulletin of Volcanology*, *74*(9), 2083–2094. https://doi.org/10.1007/s00445-012-0647-4

Cioni, R., Bertagnini, A., Santacroce, R., & Andronico, D. (2008). Explosive activity and eruption scenarios at Somma-Vesuvius (Italy): Towards a new classification scheme. *Journal of Volcanology and Geothermal Research*, *178*(3), 331–346. https://doi.org/10.1016/j.jvolgeores.2008.04.024

Clocchiatti, R., Condomines, M., Guénot, N., & Tanguy, J. (2004). Magma changes at Mount Etna: The 2001 and 2002–2003 eruptions. *Earth and Planetary Science Letters*, *226*(3–4), 397–414. https://doi.org/10.1016/j.epsl.2004.07.039

Coltelli, M., Proietti, C., Branca, S., Marsella, M., Andronico, D., & Lodato, L. (2007). Analysis of the 2001 lava flow eruption of Mt. Etna from three-dimensional mapping. *Journal of Geophysical Research*, *112*, F02029. https://doi.org/10.1029/2006JF000598

Colucci, S., de' Michieli Vitturi, M., Neri, A., & Palladino, D. (2014). An integrated model of magma chamber, conduit and column for the analysis of sustained explosive eruptions. *Earth and Planetary Science Letters*, *404*, 98–110. https://doi.org/10.1016/j.epsl.2014.07.034

Connor, L., Connor, C., Meliksetian, K., & Savov, I. (2012). Probabilistic approach to modeling lava flow inundation: A lava flow hazard assessment for a nuclear facility in Armenia. *Journal of Applied Volcanology*, *1*(1), 3. https://doi.org/10.1186/2191-5040-1-3

Coppola, D., Barsotti, S., Cigolini, C., Laiolo, M., Pfeffer, M., & Ripepe, M. (2019). Monitoring the time-averaged discharge rates, volumes and emplacement style of large lava flows by using MIROVA system: The case of the 2014-2015 eruption at Holuhraun (Iceland). *Annals of Geophysics*, *62*(2).

Coppola, D., Di Muro, A., Peltier, A., Villeneuve, N., Ferrazzini, V., Favalli, M., et al. (2017). Shallow system rejuvenation and magma discharge trends at Piton de la Fournaise volcano (La Réunion Island). *Earth and Planetary Science Letters*, *463*, 13–24. https://doi.org/10.1016/j.epsl.2017.01.024

Coppola, D., Piscopo, D., Staudacher, T., & Cigolini, C. (2009). Lava discharge rate and effusive pattern at Piton de la Fournaise from MODIS data. *Journal of Volcanology and Geothermal Research*, *184*(1-2), 174–192. https://doi.org/10.1016/j.jvolgeores.2008.11.031

Costa, A. (2005). Viscosity of high crystal content melts: Dependence on solid fraction. *Geophysical Research Letters*, *32*, L22308. https://doi.org/10.1029/2005GL024303

Costa, A., Melnik, O., & Sparks, R. (2007). Controls of conduit geometry and wallrock elasticity on lava dome eruptions. *Earth and Planetary Science Letters*, *260*(1-2), 137–151. https://doi.org/10.1016/j.epsl.2007.05.024

de' Michieli Vitturi, M., Engwell, S., Neri, A., & Barsotti, S. (2016). Uncertainty quantification and sensitivity analysis of volcanic columns models: Results from the integral model PLUME-MoM. *Journal of Volcanology and Geothermal Research*, *326*, 77–91. https://doi.org/10.1016/j.jvolgeores.2016.03.014

de' Michieli Vitturi, M., & Tarquini, S. (2017). MrLavaLoba: A new probabilistic model for the simulation of lava flows as a settling process. *Journal of Volcanology and Geothermal Research*, *349*, 323–334.
Degruyter, W., Bachmann, O., Burgisser, A., & Manga, M. (2012). The effects of outgassing on the transition between effusive and explosive silicic eruptions. *Earth and Planetary Science Letters*, *349*, 161–170.
Giordano, D., Russell, J., & Dingwell, D. (2008). Viscosity of magmatic liquids: A model. *Earth and Planetary Science Letters*, *271*(1-4), 123–134. https://doi.org/10.1016/j.epsl.2008.03.038
Got, J. L., Peltier, A., Staudacher, T., Kowalski, P., & Boissier, P. (2013). Edifice strength and magma transfer modulation at Piton de la Fournaise volcano. *Journal of Geophysical Research*, *118*, 5040–5057. https://doi.org/10.1002/jgrb.50350
Harris, A., Dehn, J., & Calvari, S. (2007). Lava effusion rate definition and measurement: A review. *Bulletin of Volcanology*, *70*(1), 1–22. https://doi.org/10.1007/s00445-007-0120-y
Harris, A., Murray, J., Aries, S., Davies, M., Flynn, L., Wooster, M., et al. (2000). Effusion rate trends at Etna and Krafla and their implications for eruptive mechanisms. *Journal of Volcanology and Geothermal Research*, *102*(3-4), 237–269. https://doi.org/10.1016/S0377-0273(00)00190-6
Harris, A., & Neri, M. (2002). Volumetric observations during paroxysmal eruptions at Mount Etna: Pressurized drainage of a shallow chamber or pulsed supply? *Journal of Volcanology and Geothermal Research*, *116*(1–2), 79–95. https://doi.org/10.1016/S0377-0273(02)00212-3
Harris, A., & Rowland, S. (2009). Effusion rate controls on lava flow length and the role of heat loss: A review. In *Studies in volcanology: The legacy of George Walker*, *Special Publications of IAVCEI* (Vol. 2, pp. 33–51). London: Geological Society.
Harris, A., Steffke, A., Calvari, S., & Spampinato, L. (2011). Thirty years of satellite-derived lava discharge rates at Etna: Implications for steady volumetric output. *Journal of Geophysical Research*, *116*, B08204. https://doi.org/10.1029/2011JB008237
Harris, A., & Stevenson, D. S. (1997). Magma budgets and steady-state activity of Vulcano and Stromboli. *Geophysical Research Letters*, *24*(9), 1043–1046. https://doi.org/10.1029/97GL00861
James, M., Pinkerton, H., & Ripepe, M. (2010). Imaging short period variations in lava flux. *Bulletin of Volcanology*, *72*(6), 671–676. https://doi.org/10.1007/s00445-010-0354-y
Kubanek, J., Westerhaus, M., & Heck, B. (2017). TanDEM-X time series analysis reveals lava flow volume and effusion rates of the 2012–2013 Tolbachik, Kamchatka fissure eruption. *Journal of Geophysical Research*, *122*, 7754–7774. https://doi.org/10.1002/2017JB014309
La Spina, G., Burton, M., & de' Michieli Vitturi, M. (2015). Temperature evolution during magma ascent in basaltic effusive eruptions: A numerical application to Stromboli volcano. *Earth and Planetary Science Letters*, *426*, 89–100. https://doi.org/10.1016/j.epsl.2015.06.015
La Spina, G., Burton, M., de' Michieli Vitturi, M., & Arzilli, F. (2016). Role of syn-eruptive plagioclase disequilibrium crystallization in basaltic magma ascent dynamics. *Nature Communications*, *7*(1), 13,402. https://doi.org/10.1038/ncomms13402
Lautze, N., Harris, A., Bailey, J., Ripepe, M., Calvari, S., Dehn, J., et al. (2004). Pulsed lava effusion at Mount Etna during 2001. *Journal of Volcanology and Geothermal Research*, *137*(1–3), 231–246. https://doi.org/10.1016/j.jvolgeores.2004.05.018
Le Métayer, O., Massoni, J., & Saurel, R. (2005). Modelling evaporation fronts with reactive Riemann solvers. *Journal of Computational Physics*, *205*(2), 567–610. https://doi.org/10.1016/j.jcp.2004.11.021
Macedonio, G., Dobran, F., & Neri, A. (1994). Erosion processes in volcanic conduits and application to the AD 79 eruption of Vesuvius. *Earth and Planetary Science Letters*, *121*(1-2), 137–152. https://doi.org/10.1016/0012-821X(94)90037-X
Macedonio, G., Neri, A., Martì, J., & Folch, A. (2005). Temporal evolution of flow conditions in sustained magmatic explosive eruptions. *Journal of Volcanology and Geothermal Research*, *143*(1-3), 153–172. https://doi.org/10.1016/j.jvolgeores.2004.09.015
Malin, M. (1980). Lengths of Hawaiian lava flows. *Geology*, *8*(7), 306–308. https://doi.org/10.1130/0091-7613(1980)8<306:LOHLF>2.0.CO;2
Marti, J., Folch, A., Neri, A., & Macedonio, G. (2000). Pressure evolution during explosive caldera-forming eruptions. *Earth and Planetary Science Letters*, *175*(3-4), 275–287. https://doi.org/10.1016/S0012-821X(99)00296-4
Melnik, O., & Sparks, R. (2005). Controls on conduit magma flow dynamics during lava dome building eruptions. *Journal of Geophysical Research*, *110*, B02209. https://doi.org/10.1029/2004JB003183
Neri, M., & Acocella, V. (2006). The 2004–2005 Etna eruption: Implications for flank deformation and structural behaviour of the volcano. *Journal of Volcanology and Geothermal Research*, *158*(1–2), 195–206. https://doi.org/10.1016/j.jvolgeores.2006.04.022
Neri, M., Acocella, V., Behncke, B., Maiolino, V., Ursino, A., & Velardita, R. (2005). Contrasting triggering mechanisms of the 2001 and 2002–2003 eruptions of Mount Etna (Italy). *Journal of Volcanology and Geothermal Research*, *144*(1–4), 235–255. https://doi.org/10.1016/j.jvolgeores.2004.11.025
Pinkerton, H., & Wilson, L. (1994). Factors controlling the lengths of channel-fed lava flows. *Bulletin of Volcanology*, *56*(2), 108–120. https://doi.org/10.1007/BF00304106
Piombo, A., Tallarico, A., & Dragoni, M. (2016). Role of mechanical erosion in controlling the effusion rate of basaltic eruptions. *Geophysical Research Letters*, *43*(17), 8970–8977. https://doi.org/10.1002/2016GL069737
Ripepe, M., Delle Donne, D., Genco, R., Maggio, G., Pistolesi, M., Marchetti, E., et al. (2015). Volcano seismicity and ground deformation unveil the gravity-driven magma discharge dynamics of a volcanic eruption. *Nature Communications*, *6*(1), 6998. https://doi.org/10.1038/ncomms7998
Ripepe, M., Delle Donne, D., Lacanna, G., Marchetti, E., & Ulivieri, G. (2009). The onset of the 2007 Stromboli effusive eruption recorded by an integrated geophysical network. *Journal of Volcanology and Geothermal Research*, *182*(3–4), 131–136. https://doi.org/10.1016/j.jvolgeores.2009.02.011
Ripepe, M., Pistolesi, M., Coppola, D., Delle Donne, D., Genco, R., Lacanna, G., et al. (2017). Forecasting effusive dynamics and decompression rates by magmastatic model at open-vent volcanoes. *Scientific Reports*, *7*(1), 3885. https://doi.org/10.1038/s41598-017-03833-3
Rose, W., Palma, J., Wolf, R., & Gomez, R. (2013). A 50 yr eruption of a basaltic composite cone: Pacaya, Guatemala. *The Geological Society of America Special Paper*, *498*, 1–21. https://doi.org/10.1130/2013.2498(01)
Saltelli, A. (2002). Making best use of model evaluations to compute sensitivity indices. *Computer Physics Communications*, *145*(2), 280–297. https://doi.org/10.1016/S0010-4655(02)00280-1
Scollo, S., Tarantola, S., Bonadonna, C., Coltelli, M., & Saltelli, A. (2008). Sensitivity analysis and uncertainty estimation for tephra dispersal models. *Journal of Geophysical Research*, *113*, B06202. https://doi.org/10.1029/2006JB004864
Smith, P., & Asimow, P. (2005). Adiabat_1ph: A new public front-end to the MELTS, pMELTS, and pHMELTS models. *Geochemistry, Geophysics, Geosystems*, *6*, Q02004. https://doi.org/10.1029/2004GC000816
Sobol, I. M. (2001). Global sensitivity indices for nonlinear mathematical models and their Monte Carlo estimates. *Mathematics and Computers in Simulation*, *55*(1-3), 271–280. https://doi.org/10.1016/S0378-4754(00)00270-6

Steffke, A., Harris, A., Burton, M., Caltabiano, T., & Salerno, G. (2011). Coupled use of COSPEC and satellite measurements to define the volumetric balance during effusive eruptions at Mt. Etna, Italy. *Journal of Volcanology and Geothermal Research*, *205*(1–2), 47–53. https://doi.org/10.1016/j.jvolgeores.2010.06.004

Swanson, D., Rose, T., Mucek, A., Garcia, M., Fiske, R., & Mastin, L. (2014). Cycles of explosive and effusive eruptions at Kīlauea Volcano, Hawaii. *Geology*, *42*(7), 631–634. https://doi.org/10.1130/G35701.1

Tallarico, A., Dragoni, M., & Zito, G. (2006). Evaluation of lava effusion rate and viscosity from other flow parameters. *Journal of Geophysical Research*, *111*, B11205. https://doi.org/10.1029/2005JB003762

Vicari, A., Ganci, G., Behncke, B., Cappello, A., Neri, M., & Del Negro, C. (2011). Near-real-time forecasting of lava flow hazards during the 12–13 January 2011 Etna eruption. *Geophysical Research Letters*, *38*, L13317. https://doi.org/10.1029/2011GL047545

Wadge, G. (1981). The variation of magma discharge during basaltic eruptions. *Journal of Volcanology and Geothermal Research*, *11*(2–4), 139–168. https://doi.org/10.1016/0377-0273(81)90020-2

Wadge, G., & Guest, J. (1981). Steady-state magma discharge at Etna 1971–81. *Nature*, *294*(5841), 548–550. https://doi.org/10.1038/294548a0

Woodhouse, M., Hogg, A., & Phillips, J. (2016). A global sensitivity analysis of the PlumeRise model of volcanic plumes. *Journal of Volcanology and Geothermal Research*, *326*, 54–76. https://doi.org/10.1016/j.jvolgeores.2016.02.019